Journal of Materials Chemistry A

Accepted Manuscript

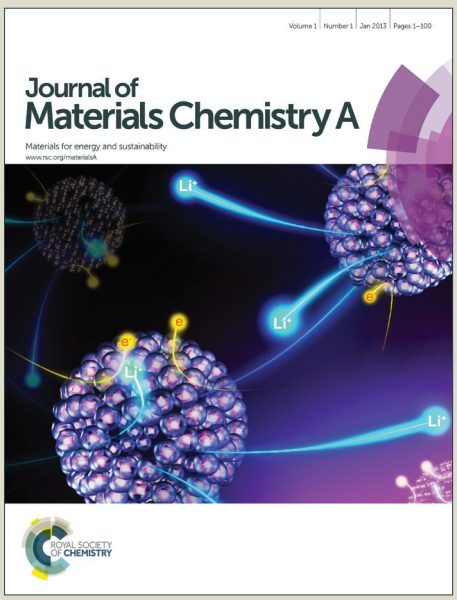

ROYAL SOCIETY OF CHEMISTRY

www.rsc.org/materialsA

Cite this: DOI: 10.1039/c0xx00000x

www.rsc.org/xxxxxx

ARTICLE TYPE

Electrospun TiO_2 Nanofibers Integrating Space-separated Magnetic Nanoparticles and Heterostructrues for Recoverable and Efficient Photocatalyst

Dahubaiyila, [a,b] Xiaohui Wang, [a,b] Xin Li [b], Baosharileaodu [b], Xiaotian Li, *[a] Liang Xu [b], Zongrui Liu [b] Limei Duan, *[b] and Jinghai Liu *[b]

Received (in XXX, XXX) Xth XXXXXXXXX 20XX, Accepted Xth XXXXXXXXX 20XX
DOI: 10.1039/b000000x

TiO_2 nanofibers integrating space-separated magnetic nanparticles and heterostructures have been fabricated to construct multifunctional photocatalysts with excellent photocatalytic activity and magnetic recoverability. Electrospinning technique has been employed to prepare the Fe_3O_4 embedded TiO_2 (Fe_3O_4@TiO_2) magnetic nanofibers. TiO_2/CdS heterostructures (Fe_3O_4@TiO_2/CdS) formed by depositing CdS nanoparticles on the Fe_3O_4@TiO_2 nanofiblers have been obtained by a hydrothermal process. The heterostrucutres improve the photocatalytic activity and widen the range in solar light response. Under the visible light irradiation, photocatalytic activity of Fe_3O_4@TiO_2/CdS nanofibers is 5.11 times higher than that of Fe_3O_4@TiO_2 nanofibers, and is 1.22 times of CdS nanoparticles. And, it exhibits a slight increase under the simulated solar light with the photocatalytic degradation ratio of 1.1 times higher than that under visible light. The loading amounts of CdS only have effects on the photocatalytic activity under visible light and simulated solar light. Besides, the Fe_3O_4@TiO_2/CdS nanofiber exhibits the saturation magnetization strength of 1.572 emu g^{-1}, and can be effortlessly separated and recovered by applying a contactless magnetic field. The cycling stability is durable after the magnetic separation and recycling.

1 Introduction

TiO_2 nanofibers are fascinating fibrous morphology nanomaterials with many applications in environmental and energy issues, such as photocatalysts [1-3], Dye-sensitized solar cells (DSSC) [4-6], Li-ion battery [7-10] and membrane filtration [11]. For applications in photocatalysis, the nanofiber morphology exhibits advantages in providing large external surface area and the inner space in the fiber to integrate functional components to construct efficient photocatalysts with high activity and recoverable separation for large scale water treatment. Electrospinning technique is a low-cost and convenient approach to fabricate the one-dimensional (1D) nanostructure and assemblies with hierarchical and core-shell structures [12-14].

Magnetic TiO_2 nanofibers as heterogeneous photocatalysts are easily separated from the reaction solution system after utilization by applying a contactless magnet. The traditional strategy to endow TiO_2 nanofibers with magnetism is to decorate the surface of the nanofibers with iron-based magnetic compounds. $CoFe_2O_4$ [15] and Fe_3O_4 [16] are loaded on the surface of the nanofibers by combining electrospinning with co-precipitation or hydrothermal treatment. However, the external surface of the TiO_2 nanofiber as a photocatalyst is extremely important to the photocatalytic activity and the construction of hierarchical heterostructures. Thus, we need to embed the magnetic functional components into the nanofiber to form a core-shell structure. The one-step electrospinning of a solution containing poly(vinyl pyrrolidone) (PVP) and alkoxide precursors of titanium and iron oxides is a direct method to achieve the embedded morphology. But, a direct contact between the embedded Fe_3O_4 and TiO_2 nanofiber would lead to the Fe^{3+}-doped TiO_2 after the calcination, which has negative effects on the photocatalytic activity. An approach to resolve this problem is to coat the magnetic iron oxide nanoparticles with an isolating shell. Silica (SiO_2) is usually chosen as a versatile shell in the configuration of the core-shell structure. The extended Stöber method has been applied to fabricate a uniform and porous SiO_2 shell on magnetic Fe_3O_4 core [17-19]. This technique paves the way for constructing embedded magnetic Fe_3O_4 inside the TiO_2 nanofiber by direct electrospinning of the mixed dispersion of precursors, Fe_3O_4 with SiO_2 shell and PVP solution.

Heterostructrues design on the surface of TiO_2 nanofibers is an effective means to improve the photocatalytic activity by forming heterojunctions. Semiconductors, plasmonic nanoparticles and photosensitive metal complexes are deposited or assembled on the TiO_2 nanofibers to form heterojunctions, such as $SrTiO_3$ [1a], SnO_2 [20-22], SnS_2 [23], WO_3 [24], $Ba_4Ti_3O_{12}$ [25], CeO_2 [26], In_2O_3 [27], V_2O_5 [28], Ag and Au nanoparticles [29, 30] and copper (II) phthalocyanine [31]. CdS is a typical narrow band gap semiconductor with a band gap of 2.4 eV and a more negative conduction band (C.B.) electrochemical potential than that of TiO_2 [32, 33]. When the CdS/TiO_2 composite is exposed to the low energy photons of visible light, in principle, the electrons which are photo-excited to

the C.B. of CdS are transferred to that of TiO_2. Accordingly, the electrons and holes produced in CdS/TiO_2 heterostructure are separated and its spectrum response is extended to visible light, which could contribute to improve the catalytic activity.

Herein, we reported the fabrication of TiO_2 nanofibers integrating embedded magnetic Fe_3O_4 nanoparticles and TiO_2/CdS heterostructures as efficient photocatalysts with magnetic recoverability. The Fe_3O_4 embedded TiO_2 (Fe_3O_4@TiO_2) magnetic nanofibers were prepared through electrospinning process combined with heat treatment at 753 K. The CdS nanoparticles were then deposited on the surface of Fe_3O_4@TiO_2 nanofibers (Fe_3O_4@TiO_2/CdS nanofiber) through a hydrothermal process. The XRD pattern shows that TiO_2 nanofibers are converted to anatase phase after heat treatment. The characteristic SEM and TEM morphologies directly illustrate that the Fe_3O_4 nanoparticles are completely encapsulated in TiO_2 nanofibers with the CdS nanoparticles well dispersed on the surface. The UV-Vis diffuse reflectance spectra (UV-Vis DRS) show that the light absorption of Fe_3O_4@TiO_2/CdS nanofiber is enhanced, and adsorption edge is extended to the visible spectrum range. The photocatalytic degradation ratio of Fe_3O_4@TiO_2/CdS-3 nanofibers for Rhodamine B (RhB) is 97.65% under UV irradiation, which is similar to the control sample of TiO_2 nanofibers with photocatalytic degradation ratio of 92.06% and Fe_3O_4@TiO_2 nanofibers with the one of 97.86%. Under the visible light irradiation, photocatalytic activity of Fe_3O_4@TiO_2/CdS nanofibers is 5.11 times higher than that of Fe_3O_4@TiO_2 nanofibers, and is 1.22 times of CdS nanoparticles. And, it exhibits a slight increase under the simulated solar light with the photocatalytic degradation ratio of 1.1 times higher than that under visible light. The loading amounts of CdS only have effects on the photocatalytic activity under visible light and simulated solar light. Besides, Fe_3O_4@TiO_2/CdS nanofibers exhibit strong magnetism and can be easily separated and recovered by adding a contactless magnetic field. The cycling stability is durable after the magnetic separation and recycling.

2 Materials and Methods

2.1 Preparation of Fe_3O_4@SiO_2 core-shell structure

Fe_3O_4 nanoparticles were prepared by solution precipitation according to the literature [34]. $FeCl_3.6H_2O$ (1.817g, analytic purity, Sonochemical Sinopharm Chemical Reagent Co., Ltd) was mixed with $FeCl_2.4H_2O$ (1.113g, analytic purity, Sonochemical Sinopharm Chemical Reagent Co., Ltd) under N_2 atmosphere to react for 5 hours at 50 ^oC. After 0.5 hour, concentrated ammonia (15ml, analytic purity, Sonochemical Sinopharm Chemical Reagent Co., Ltd) was added to precipitate the Fe_3O_4. For the preparation of Fe_3O_4@SiO_2, 0.4 g Fe_3O_4 was added in the mixed solution containing 80 mL absolute ethanol (analytic purity, Sonochemical Sinopharm Chemical Reagent Co., Ltd) and 20 mL deionized water. After ultrasonic dispersion, 1mL of concentrated ammonia (28 wt%) was added into the solution. The mixed solution was stirred and, at the same time, 0.6 mL tetraethyl orthosilicate (analytic purity, Sonochemical Sinopharm Chemical Reagent Co., Ltd) and 5 mL absolute ethanol were added into the mixed solution which was stirred constantly in the water bath at 30 ^oC for 8 h. The product was recovered with a magnet and washed with deionized water and absolute ethanol three times, followed by drying at 80 for 2 h in vaccum oven.

2.2 Preparation of magnetic Fe_3O_4@TiO_2 nanofibers

1.5 g PVP (MW 1300000, Aladdin Chemistry Co. Ltd) was dissolved in 15 mL anhydrous ethanol (> 99 wt%) and stirred until the solution turned transparent. 0.1 g Fe_3O_4@SiO_2 nanoparticles were added into the above solution. After ultrasound treatment, the dispersion was intensively stirred for 24 h. The obtained dispersion was signed as A. 2 mL tetrabutyl ortho titanate was added dropwise into the mixed solution of 4 mL anhydrous ethanol and 4 mL acetic acid (99.5%). The mixed solution was stirred for 30 min, and the formed yellow solution named B. Solution B was slowly added into A and strongly stirred for 4 h. The above gel was injected into a syringe of the self-made electrospinning apparatus with a copper electrode that inserted into the syringe. Then aluminum foil as cathode was placed in front of the nozzle with a distance of 20 cm and operated at 9 kV. After 10 h, a large fiber mat was produced. After hydrolyzing completely in the air, the products were dried under vaccum at 80 ^oC for 4 h. The products were then heated in a muffle furnace with heating rate of 1 ^oC/min from room temperature to 480 ^oC and kept at 480 ^oC for 10 h to obtain Fe_3O_4@TiO_2 nanofibers.

2.3 Integrating TiO_2/CdS heterostructures on Fe_3O_4@TiO_2 nanofibers (Fe_3O_4@TiO_2/CdS)

The Fe_3O_4@TiO_2/CdS nanofibers were synthesized by a hydrothermal method. Three portions (each 0.050 g) of magnetic Fe_3O_4@TiO_2 nanofibers were added into the three reaction solutions composed of 20 mL of deionezed water (DI water), cadmium acetate and thiourea with the molar ratio of cadmium acetate and thiourea of 1:3, while the cadmium acetate are 0.1 mmol, 0.5 mmol and 0.8 mmol, respectively. The three solutions were transferred to Teflon-lined stainless autoclaves. The hydrothermal treatment was conducted at 130 ^oC for 12 h and then cooled at room temperature. The magnetic products were collected by a magnet, and were washed with DI water and ethanol three times followed by drying at 80 ^oC for 12 h. The obtained products were denoted as Fe_3O_4@TiO_2/CdS-1, Fe_3O_4@TiO_2/CdS-2, and Fe_3O_4@TiO_2/CdS-3 nanofibers.

2.4 Characterization

X-ray diffraction (XRD) patterns were recorded on a D8 Tool diffractometer using Cu Ka (λ=0.15418 nm). SEM images were performed on a JEOL JSM-6700F field emission scanning electron microscope. The TEM images were observed on H-7650 transmission electron microscope operated at 120 kV. UV-Vis diffuse reflectance spectra (DRS) were recorded on a DWS 003 spectrophotometer. The magnetization curve was obtained on LaKe Shole7304 ibrating Sample Magnetometer (VSM). The concentration of cadmium ion (Cd^{2+}) in the solution was tested on a prodigty XP ICP-AES.

2.5 Adsorption and photocatalytic process

The photocatalytic activity was tested by examining the degradation of RhB in aqueous solution. The ultraviolet (UV) light was illuminated by a 50 W high-pressure mercury lamp. Visible light and simulated solar light were illuminated by a Xe

lamp with UV cut-off filter and simulated solar light filter. Samples (0.010 g and 0.020 g) was added into 100 mL of the new prepared Rhodamine B (RhB) solution (1.0×10^{-5} mol L^{-1}) and stirred for 10 min at room temperature to obtain a good dispersion. Then, the system was kept in the dark to reach saturation adsorption for 1 hour. The irradiation started and the reaction system temperature was kept at 23±3 °C by water cooling. After centrifugation to remove the photocatalyst, the concentration of RhB in the solution was measured by UV-Vis spectroscopy.

3. Results and discussion

The crystalline phase of the as-prepared samples was analyzed by powder X-ray diffraction (XRD). Fig.1 presents the XRD pattern of Fe_3O_4 nanoparticles, Fe_3O_4@TiO_2 nanofibers, and the CdS deposited Fe_3O_4@TiO_2 nanofibers (Fe_3O_4@TiO_2/CdS-2 nanofibers). All of the diffraction peaks in Fig. 1a can be indexed to the Fe_3O_4 structure (JCPDS 75-1609) which illustrate a high purity and crystallinity of the prepared Fe_3O_4 nanoparticles. As shown in Fig. 1b, the intensity of the Fe_3O_4 diffraction peaks weakens apparently and the identified peak at 25.4° is in good agreement with that of anatase TiO_2. The result in Fig. 1c shows the characteristic peaks of CdS at 26.80°, 28.08°, 43.90° and 52.20° (2θ), which is corresponded to (002), (101), (110) and (201) crystal faces and agreed with the standard peaks of hexagonal crystal of CdS (JCPDS 10-077-2306). According to the Scherrer equation, the average CdS particle size along (002) is 16.08 nm. Therefore, it is concluded that integration of magnetic nanoparticles and heterostructures on the Fe_3O_4@TiO_2/CdS nanofibers were successfully fabricated by the combination of an electrospinning technique with a hydrothermal synthesis.

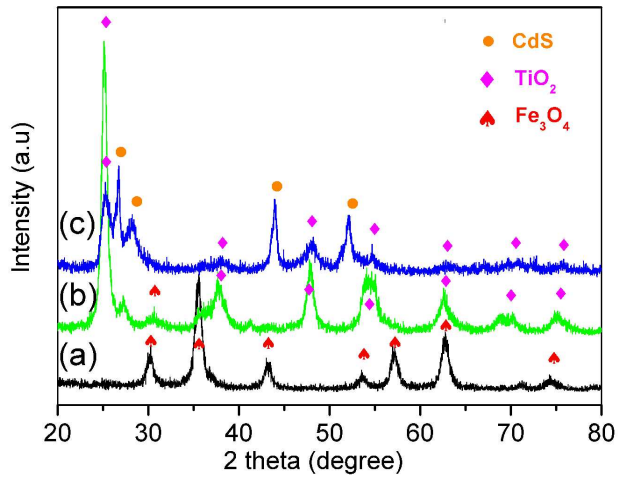

Fig.1 XRD pattern of the electrospun TiO_2 nanofibers integrating space-separated magnetic Fe_3O_4 nanoparticles and TiO_2/CdS heterostructures. (a) Fe_3O_4 nanoparticles. (b) Fe_3O_4@TiO_2 nanofibers. (c) Fe_3O_4@TiO_2/CdS-2 nanofibers.

Magnetic nanoparticles and heterostructures space-separated morphology of the Fe_3O_4@TiO_2/CdS nanofibers with different CdS loading amounts was examined. Fig. 2 shows typical scanning electron microscopy (SEM) images. It can be clearly seen in Fig. 2a that the diameter of uniform nanofibers is in the range of 150-200 nm. The surface of Fe_3O_4@TiO_2 nanofiber is relatively smooth with fiber lengths above 10 μm. The scanning electron microscope (SEM) images from Fig. 2b to Fig. 2d reveal that Fe_3O_4@TiO_2/CdS nanofibers are composed of numerous highly dispersed CdS nanoparticles with size of 15 nm attached onto the surface of the Fe_3O_4@TiO_2 nanofiber, thus resulting in the hierarchical heterostructures with a rough surface. To investigate the effects of CdS loading amounts on the photocatalytic activity, we have prepared Fe_3O_4@TiO_2/CdS nanofibers with different CdS loading amounts. As the concentrations of cadmium acetate and thiourea increase under the hydrothermal process, the loading amount of CdS on the Fe_3O_4@TiO_2 nanofiber increases. The results in Fig. 2c exhibit that when the amount of CdS reaches 59.1 wt%, the fiberous morphology is well retained with a little increase in the diameter due to CdS nanoparticles loading and with a rough surface. When the amount of CdS reaches 70.0 wt%, the loading density of CdS nanoparticles on nanofibers increases, and simultaneously the aggregation of CdS nanoparticles occurs, as shown in Fig. 2d.

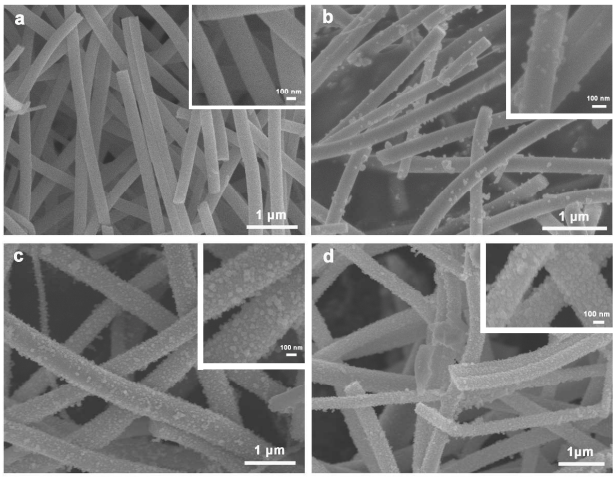

Fig. 2 SEM images of the electrospun TiO_2 nanofibers integrating space-separated magnetic Fe_3O_4 nanoparticles and TiO_2/CdS heterostructure. (a) Fe_3O_4@TiO_2 nanofibers. (b) Fe_3O_4@TiO_2/CdS-1 nanofibers with CdS 22.4 wt%. (c) Fe_3O_4@TiO_2/CdS-2 nanofibers with CdS 59.1 wt%. (d) Fe_3O_4@TiO_2/CdS-3 nanofibers with CdS 70.0 wt%.

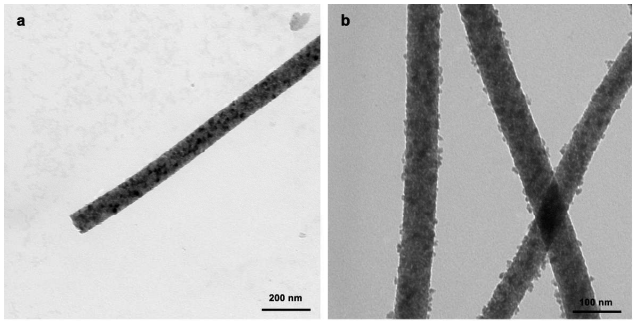

Fig.3 TEM images of the electrospun TiO_2 nanofibers integrating space-separated magnetic Fe_3O_4 nanoparticles and TiO_2/CdS heterostructures. (a) Fe_3O_4@TiO_2 nanofibers. (b) Fe_3O_4@TiO_2/CdS-2 nanofibers

Transmission electron microscopy (TEM) has been used to investigate the functional components space-separated morphology of the typical Fe_3O_4@TiO_2/CdS-2 nanofibers. As shown in Fig. 3a, it can be observed that the surface of the

nanofiber appears smooth, and Fe_3O_4@SiO_2 nanoparticles were uniformly embedded in the nanofibers. The TEM images in Fig. 3b clearly show the rough surface of Fe_3O_4@TiO_2/CdS nanofibers with small branches. They are the uniformly dispersed CdS nanoparticles, which is in accordance with the SEM image of Fig. 2c.

Fig. 4 shows the UV-Vis diffuse reflectance spectra (UV-Vis DRS) of the electrospun TiO_2 nanofibers with embeedd magnetic Fe_3O_4 nanoparticles and surface CdS heterostructures. The light absorption of Fe_3O_4@TiO_2/CdS nanofibers is extended to 510 nm, and the absorption edge shows an apparent red-shift. Moreover, its absorption intensity is enhanced by comparasion with magnetic Fe_3O_4@TiO_2 nanofibers. This result indicates that the photo-response range after CdS surface deposition is extended and photoabsorption ability is enhanced.

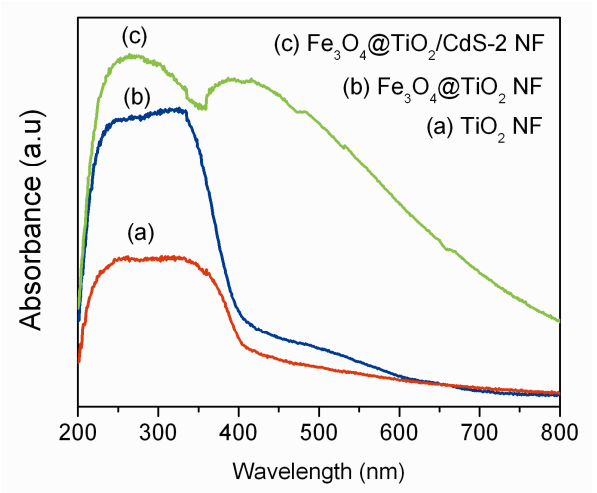

Fig.4 UV-Vis diffuse reflectance spectra (UV-Vis DRS) of the electrospun TiO_2 nanofibers integrating space-separated magnetic Fe_3O_4 nanoparticles and TiO_2/CdS heterostructures. (a) TiO_2 nanofibers (TiO_2 NF). (b) Fe_3O_4@TiO_2 nanofibers (Fe_3O_4@TiO_2 NF). (c) Fe_3O_4@TiO_2/CdS-2 nanofibers (Fe_3O_4@TiO_2/CdS-2 NF).

Photocatalytic activities of Fe_3O_4@TiO_2/CdS nanofibers with different CdS loading amounts were investigated through examining the degradation of RhB in aqueous solution (See Fig. S1, ESI†). The adsorption and photocatalytic activity of Fe_3O_4@TiO_2/CdS nanofibers under UV light, visible light and simulated solar light were also examined by employing TiO_2 nanofibers, Fe_3O_4@TiO_2 nanofibers and CdS nanoparticles as control to justify the contribution of heterostructures to the Fe_3O_4@TiO_2/CdS nanofibers. The results in Fig. 5a and Table 1 (See ESI†) show that the CdS on the surface of Fe_3O_4@TiO_2 nanofibers has little effects on the increase of photocatalytic activity under UV irradiation. The photocatalytic degradation ratio of Fe_3O_4@TiO_2/CdS-3 nanofibers for RhB is 97.65%, which is similar to the control sample of TiO_2 nanofibers with photocatalytic degradation ratio of 92.06% and Fe_3O_4@TiO_2 nanofibers with the one of 97.86%. And, the variable CdS loading amounts for Fe_3O_4@TiO_2/CdS-1 and Fe_3O_4@TiO_2/CdS-2 nanofibers also exhibit little contribution to the photocatalytic activity under UV irradiation.

We consider that the reason would be ascribed to unexcited CdS under UV irradiation, and the photocatalytic activity is derived from TiO_2 nanofibers. To further investigate this hypothesis, we carried out adsorption and photocatalytic experiments for Fe_3O_4@TiO_2/CdS nanofibers under visible light and simulated solar light by using CdS nanoparticles, Fe_3O_4@TiO_2 nanofibers and TiO_2 nanofibers as control. The results in Fig. 5b show that the photocatalytic activity of Fe_3O_4@TiO_2/CdS nanofibers is 5.11 times higher than that of Fe_3O_4@TiO_2 nanofibers, and is 1.22 times of CdS nanoparticles. The increased photocatalytic activity of Fe_3O_4@TiO_2/CdS nanofibers under visible light irradiation is ascribed to the heterojunctions between the TiO_2 nanofibers and CdS nanoparticles, which benefits the separation of excited holes and electrons. Besides, the photocatalytic degradation ratio of Fe_3O_4@TiO_2/CdS nanofibers for RhB ascends from 71.27% to 90.25% as the loading amounts of CdS nanoparticles increases from 22.4wt% for Fe_3O_4@TiO_2/CdS-1 to 70.0 wt% for Fe_3O_4@TiO_2/CdS-3.

To further demonstrate the roles of heterostructures in improving the photocatalytic activity and widening the range of solar light response, we have also compared the activity of Fe_3O_4@TiO_2/CdS for degrading RhB solution under the irradiation of simulated solar light with that under visible light. The Fig. 5c shows that the Fe_3O_4@TiO_2/CdS nanofibers as photocatalysts exhibit higher photocatalytic degradation ratio for RhB under simulated solar light irradiation. The photocatalytic activity of Fe_3O_4@TiO_2/CdS nanofibers is 1.68 times higher than that of Fe_3O_4@TiO_2 nanofibers, and is 1.36 times of CdS nanoparticles. Moreover, the photocatalytic degradation ratio of Fe_3O_4@TiO_2/CdS nanofibers for RhB ascends from 71.61% to 92.55% as the loading percent of CdS nanoparticles increases from 22.4wt% for Fe_3O_4@TiO_2/CdS-1 to 70.0 wt% for Fe_3O_4@TiO_2/CdS-3. The photocatalytic degradation ratio of Fe_3O_4@TiO_2 nanofibers for RhB is 3.6 times of that under visible light irradiation. In contrast with the CdS control, Fe_3O_4@TiO_2/CdS nanofibers exhibit a slight increase in photocatalytic activity under the simulated solar light with photocatalytic degradation ratio of 1.1 times higher than that under visible light irradiation.

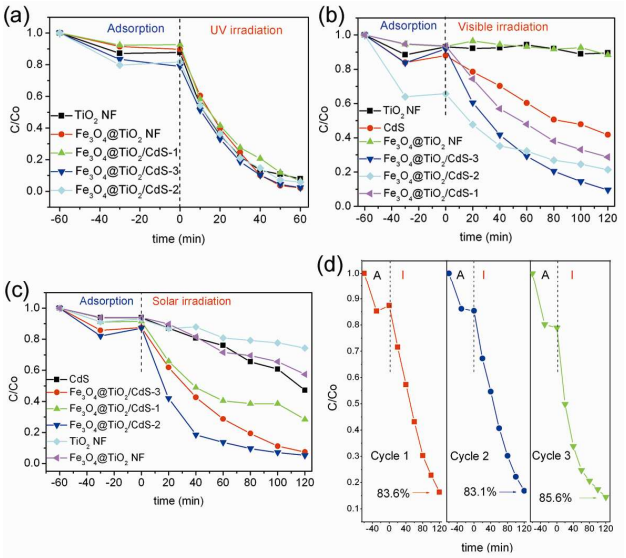

Fig.5 Adsorption and photocatalytic activity of the electrospun TiO_2 nanofibers integrating space-separated magnetic Fe_3O_4 nanoparticles and TiO_2/CdS heterostructure (Fe_3O_4@TiO_2/CdS) for degradation of RhB.

Fe_3O_4@TiO_2/CdS-1 with CdS 22.4wt%, Fe_3O_4@TiO_2/CdS-2 with CdS 59.1wt% and Fe_3O_4@TiO_2/CdS-3 with CdS 70.0 wt%. (a) UV irradiation (High pressure Hg lamp) with TiO_2 nanofibers (TiO_2 NF), Fe_3O_4@TiO_2 nanofibers (Fe_3O_4@TiO_2 NF) as control. (b) Visible light irradiation (Xe lamp with visible light cut-off filter (>400 nm)) with CdS nanoparticles, TiO_2 nanofibers (TiO_2 NF), Fe_3O_4@TiO_2 nanofibers (Fe_3O_4@TiO_2 NF) as control. (c) Solar light irradiation (Xe lamp with simulated solar light filter) with CdS nanoparticles, TiO_2 nanofibers (TiO_2 NF), Fe_3O_4@TiO_2 nanofibers (Fe_3O_4@TiO_2 NF) as control. (d) Cycling stability of Fe_3O_4@TiO_2/CdS-3 NF under solar light irradiation (Xe lamp with simulated solar light filter) (A: adsorption and I: irradiation under solar light). The minus value in the time axis denotes the adsorption in the dark.

The cycling stability of Fe_3O_4@TiO_2/CdS nanofibers as a magnetically recoverable photocatalyst was also investigated. As shown in Fig. 5d, adsorption in the dark and photocatalytic activity under simulated solar light irradiation are retainable during the 3 cycles. But, photocatalytic degradation ratio of Fe_3O_4@TiO_2/CdS nanofibers for RhB decreases from 85.6% at 3th cycle to 61.8% at 5th cycle (See Fig. S2, ESI†).

As a concern that cadmium ion (Cd^{2+}) would remain in the solution after the adsorption and photocatalytic process, we have checked the Cd^{2+} in the solution by ICP-AES after separating the powder photocatalysts with a high speed centrifugation. Under the same adsorption and irradiation conditions for the Fe_3O_4@TiO_2/CdS-3 nanofibers with CdS 70 wt% and the CdS control, The Cd^{2+} concentration (C_{Cd}^{2+}) in the solution after adsorption and simulated solar light irradiation is 56.86 mg L^{-1} for CdS control and 53.2 mg L^{-1} for Fe_3O_4@TiO_2/CdS-3 nanofibers. Fortunately, the C_{Cd}^{2+} in the solution declines during the following cycles, and it decreases to 9.7 mg L^{-1} after the 4th cycle (See Fig. S3, ESI†).

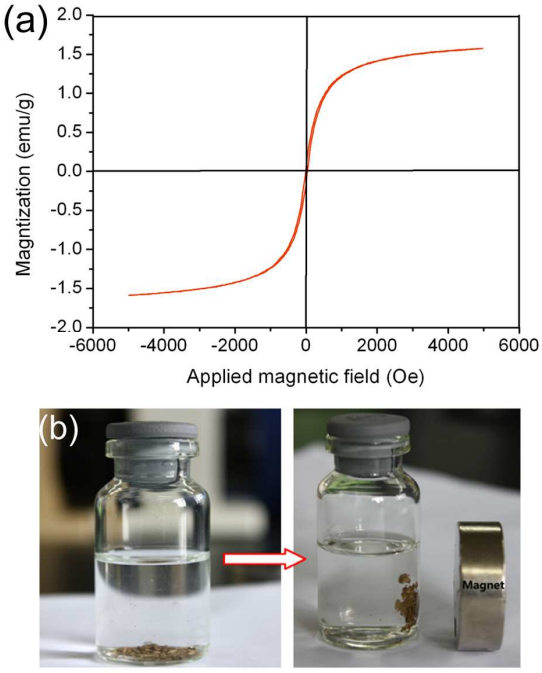

Fig.6 Magnetization and magnetic field induced separation and recoverability of Fe_3O_4@TiO_2/CdS nanofibers. (a) Magnetization curve of Fe_3O_4@TiO_2/CdS nanofibers. (b) Photo images of separation and recoverability of Fe_3O_4@TiO_2/CdS nanofibers by a contactless magnet.

Magnetization curve of Fe_3O_4@TiO_2/CdS nanofibers exhibits near-zero coercivity and remanence, suggesting a super paramagnetic nature as shown in Fig. 6a. The saturation magnetization strength is 1.572 emu g^{-1}. It can be separated and recovered by applying a contactless magnetic field. As shown in Fig. 6b, the Fe_3O_4@TiO_2/CdS nanofibers were separated and collected from the solution with a magnet placed outside the bottle. Comparatively, the technology of contactless magnetic separation is easier to operate than the methods of traditional filter and centrifugal separation, and shows a promising potential in large scale industrial application.

Conclusions

In this work, anatase TiO_2 nanofibers integrating space-separated magnetic Fe_3O_4 nanoparticles and TiO_2/CdS heterostructrues with magnetic recoverability and enhanced photocatalytic activity have been fabricated. Magnetic Fe_3O_4 nanopartilces with SiO_2 shells have been successfully embedded in the TiO_2 nanofiber (Fe_3O_4@TiO_2) through an electrospinning process. TiO_2/CdS heterostructures constructed by depositing CdS nanoparticles on the surface of Fe_3O_4@TiO_2 nanofiber has been formed through a hydrothermal process. The heterostructures increases the photocatalytic activity of the Fe_3O_4@TiO_2/CdS nanofibers, and the loading amounts of CdS nanoparticles only show positive effects on the photocatalytic activity under visible light and simulated solar light irradiation. The embedded magnetic Fe_3O_4 nanopartilces allow the integrated Fe_3O_4@TiO_2/CdS nanofibers to be effortlessly separated and recovered by applying a magnet. The strategy of integrating space-separated functional components on nanofibers provides a promising approach to design multifunctional components integration on fibrous morphology towards advanced photocatalysts with higher activity, effortless recoverability and durable recyclability.

Acknowledgements

We thank the funding support from the National Natural Science Funding of China (21076094, 21061010, 21261014 and 21303080). Natural Science Foundation of Inner Mongolia (2013MS0211, 2013MS0216). Open project from Key Laboratory of Nanodevices and Applications, Suzhou Institute of Nano-Tech and Nano-Bionics, Chinese Academy of Sciences (13ZS03). Cooperative Project of Tongliao-IMUN (SXYB2012027, SXYB2012072). Ph.D Initiative Science Foundation of Inner Mongolia University for the Nationalities (BS288). Science Foundation of Inner Mongolia University for the Nationalities (NMD1314).

Notes and references

[a] *Department of Material Science and Engineering, Jilin University, Chuangchun, 130012, P. R. China.*
E-mail: xiaotianli@jlu.edu.cn
[b] *Institute of Functional Materials, College of Chemistry and Chemical Engineering, Inner Mongolia University for The Nationalities, Tongliao, 028000, P. R. China.. Fax +86 (0)475-8313162: Tel: +86 (0)475-8251135;*
E-mail: jhliu2008@sinano.ac.cn; duanlmxie@126.com

† Electronic Supplementary Information (ESI) available: [**Fig.S1** UV-Vis absorption of RhB during photocatalytic process. **Fig.S2** Cycling performances of adsorption and photocatalytic activity of Fe_3O_4@TiO_2/CdS-3 nanofibers. **Fig.S3** Cadmium ion (Cd^{2+})

concentration (C_{Cd2+}) in the solution. **Table 1** Comparison of adsorption and photocatalytic activity of Fe_3O_4@TiO_2/CdS nanofiber (NF) and control samples.]. See DOI: 10.1039/b000000x/

1 (a) T. P. Cao, Y. J. Li，C. H. Wang, C. L. Shao, Y. C. Liu，*Langmuir*, 2011, **27**, 2946. (b) J. W. Fu, S. W. Cao, J.G. Yu, J. X. Low, Y. P. Lei, *Dalton Trans.*, 2014, DOI: 10.1039/C4DT00181H. (c) W. H. Ryu, Y. W. Lee, Y. S. Nam, D. Y. Youn, C. B. Park, Il-D. Kim, *J. Mater. Chem. A*, 2014,**2**, 5610-5615. (d) K. Liu, Y. C. Hsueh, H. S. Chen, T. P. Perng, *J. Mater. Chem. A*, 2014, **2**, 5387-5393.

2 (a) Y. H. Yang, J. W. Wen, J. H. Wei, R. Xiong, J. Shi, C. X. Pan, *ACS Appl. Mater. Interfaces*, 2013, **5** , 6201. (b) X. Zhang, X. Li, C. Shao, J. Li, M. Zhang, P. Zhang, K. Wang, N. Lu, Y. Liu, *J. Hazard. Mater.*, 2013, **260**, 892-900. (c) Z. Y. Zhang, A. R. Li, S. W. Cao, M. Bosman, S. Z. Li, C. Xue, *Nanoscale*, 2014, **6**, 5217-5222. (d) Y. Q. Dai, Y. B. Sun, J. Yao, D. D. Ling, Y. M. Wang, H. Long, X. T. Wang, B. P. Lin, T. Y. Helen Zeng, Y. M. Sun, *J. Mater. Chem. A*, 2014, **2**, 1060-1067.

3 (a) H. P. Li, W. Zhang, B. Li, W. Pan, *J. Am. Ceram. Soc.*, 2010, **93**, 2503. (b) W. Li, Y. Bai, W. Zhuang, K. Y. Chan, C. Liu, Z. H. Yang, X. Feng, X. H. Lu, *J. Phys. Chem. C*, 2014, **118**, 3049–3055. (c) Z. D. Li, C. H. Yao, Y. H. Yu, Z. Y. Cai, X. D. Wang, *Adv. Mater.*, 2014, DOI: 10.1002/adma.201303369. (d) L. Zhang, D. W. Jing, X. L. She, H. W. Liu, D. J. Yang, Y. Lu, J. Li, Z. F. Zheng, L. J. Guo, *J. Mater. Chem. A*, 2014, **2**, 2071-2078.

4 E. Ghadiri, N. Taghavinia, S. M. Zakeeruddin, M. Grätzel, J.-E. Moser, *Nano Lett.*, 2010, **10** ,1632.

5 D. Regonini, A. C. Teloeken, A. K. Alves, F. A. Berutti, K. Gajda-Schrantz, C. P. Bergmann, T. Graule, and F. Clemens, *ACS Appl. Mater. Interfaces*, 2013, **5**, 11747.

6 X. X. Wang, G. F. He, H. Fong, Z. T. Zhu, *J. Phys. Chem. C*, 2013, **117**, 1641.

7 H. Han, T. Song, J.-Y. Bae, L. F. Nazar, H. Kim, U. Paik, *Energy Environ. Sci.*, 2011, **4**, 4532.

8 J. Choi, S. Lee, J. Ha, T. Song, U. Paik, *Nanoscale*, 2013, **5**, 3230.

9 V. Aravindan, J. Sundaramurthy, P. S. Kumar, N. Shubha, W. C. Ling, S. Ramakrishna, S. Madhavi, *Nanoscale*, 2013,**5**, 10636.

10 X. Zhang, P. S. Kumar, V. Aravindan, H. H. Liu, J. Sundaramurthy, S. G. Mhaisalkar, H. M. Duong, S. Ramakrishna, S. Madhavi, *J. Phys. Chem. C*, 2012, **116**, 14780.

11 V. Thavasi, G. Singh, S. Ramakrishna, Energy Environ. Sci., 2008, 1, 205–221.

12 (a) Z. Y. Zhang, C. L. Shao, X. H. Li, L. Zhang, H. M. Xue, C. H. Wang, Y. C. Liu, *J. Phys. Chem. C*, 2010, **114**, 7920. (b) Z. Y. Zhang, C. L. Shao, X. H. Li, C. H. Wang, M. Y. Zhang, Y. C. Liu, *ACS Appl. Mater. Interfaces*, 2010, **2**, 2915.

13 D. Li, Y. N. Xia, *Nano Letters*, 2003, **3**, 555.

14 (a) R. Ostermann, D. Li, Y. D. Yin, J. T. McCann, Y. N. Xia, *Nano Letters*, 2006, **6**, 1297. (b) Z. Lou, F. Li, J. N. Deng, L. L. Wang, T. Zhang, *ACS Appl. Mater. Interfaces*, 2013, **5**, 12310.

15 (a) V. Pongsorrarith, C. Srisitthiratkul, K. Laohhasurayotin, N. Intasant, *Materials Letters*, 2012, **67**, 1. (b) C. J. Li, J. N. Wang, B. Wang, J. R. Gong, Z. Lin, *Materials Research Bulletin*, 2012, **47**, 333.

16 H. G. Wang, X. L. Fei, L. Wang, Y. P. Li, S. F. Xu, M. D. Sun, L. Sun, C. Q. Zhang, Y. X. Li, Q. B. Yang, Y. Wei, *New J. Chem.*, 2011, **35**, 1795.

17 W. Li, D. Y. Zhao, *Adv. Mater.*, 2013, **25**, 142.

18 W. R. Zhao, J. L. Gu, L. X. Zhang, H. R. Chen, J. L. Shi, *J. Am. Chem. Soc.*, 2005, **127**, 8916.

19 Y. H. Deng , D. W. Qi , C. H. Deng , X. M. Zhang , D. Y. Zhao, *J. Am. Chem. Soc.*, 2008 , **130**, 28.

20 Z. Liu, D.D. Sun, P. Guo, J.O. Leckie, *Nano Letters*, 2007, **7**, 1081.

21 C. H. Wang, C. L. Shao, X. T. Zhang, Y. C. Liu, *Inorg. Chem.*, 2009, **48**, 7261.

22 R. Zhang, H. Wu, D. D. Lin, W. Pan, *J. Am. Ceram. Soc.*, 2009, **92**, 2463.

23 Z. Y. Zhang, C. L. Shao, X. H. Li, Y. Y. Sun, M. Y. Zhang, J. B. Mu, P. Zhang, Z. C. Guo, Y. C. Liu, *Nanoscale*, 2013,**5**, 606.

24 L. Zhang, Y. G. Li, Q. H. Zhang, H. Z. Wang, *CrystEngComm,* 2013, **15**, 5986.

25 T. P. Cao, Y. J. Li, C. H. Wang, Z. Y. Zhang, M. Y. Zhang, C. L. Shao, Y. C. Liu, *J. Mater. Chem.*, 2011, **21**, 6922.

26 T. P. Cao, Y. J. Li, C. H. Wang, L. M. Wei, C. L. Shao, Y. C. Liu, *Materials Research Bulletin*, 2010, **45**, 1406.

27 J. B. Mu, B. Chen, M. Y. Zhang, Z. C. Guo, P. Zhang, Z. Y. Zhang, Y. Y. Sun, C. L. Shao, Y. C. Liu, *ACS Appl. Mater. Interfaces*, 2012, **4**, 424.

28 Y. Wang, Y. R. Su, L. Qiao, L. X. Liu, Q. Su, C. Q. Zhu, X. Q. Liu, *Nanotechnology*, 2011, **22**, 225702.

29 P. Zhang, C. L. Shao, X. H. Li, M. Y. Zhang, X. Zhang, Y. Y. Sun, Y. C. Liu, *Journal of Hazardous Materials*, 2012, **237-238**, 331.

30 S. H. Xuan, Y. J. Wang, J. C. Yu, K. C. Leung, *Langmuir*, 2009, **25**,11835.

31 M. Y. Zhang, C. L. Shao, Z. C. Guo, Z. Y. Zhang, J. B. Mu, T. P. Cao, Y. C. Liu, *ACS Appl. Mater. Interfaces*, 2011, **3**, 369.

32 R. Marschall, *Adv. Funct. Mater.* , 2013, DOI: 10.1002/adfm.201303214.

33 L. Y. Mao, Y. R. Wang, Y. J. Zhong, J. Q. Ning, Y. Hu, *J. Mater. Chem. A*, 2013, **1**, 8101.

34 Z. L. Liu, Y. J. Liu, K. L. Yao, Z. H. Ding, J. Tao, X. Wang, *J. Mater. Synth. Process.*, 2002, **10**, 83.

Table of Content (TOC):

Electrospun TiO_2 Nanofibers Integrating Space-separated Magnetic Nanoparticles and Heterostructrues for Recoverable and Efficient Photocatalyst

Dahubaiyila, Xiaohui Wang, Xin Li, Baosharileaodu, Xiaotian Li*, Liang Xu, Zongrui Liu, Limei Duan* and Jinghai Liu *

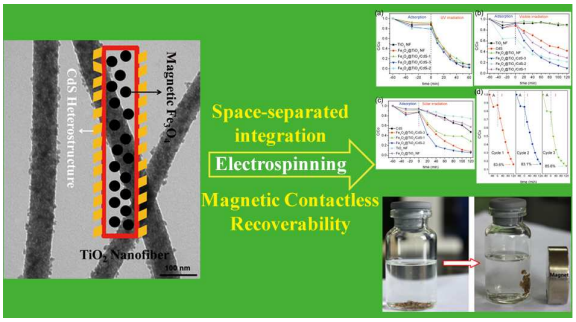

TiO_2 nanofibers integrating space-separated magnetic Fe_3O_4 nanparticles and TiO_2/CdS heterostructure (Fe_3O_4@TiO_2/CdS nanofiber) have been fabricated to construct multifunctional photocatalyst with excellent photocatalytic activity and magnetic recoverability. The heterostrucutres improve the photocatalytic activity and widen the range in solar light response. The loading amounts of CdS only have effects on the photocatalytic activity under visible light and simulated solar light. Besides, the Fe_3O_4@TiO_2/CdS nanofibers exhibit strong magnetism and can be effortlessly separated and recovered by applying a simple contactless magnetic field. The cycling stability is durable after the magnetic separation and recycling.